JOURNAL OF AIRCRAFT
Vol. 46, No. 5, September–October 2009

Numerical Analysis on Aerodynamic Force Generation of Biplane Counter-Flapping Flexible Airfoils

Jr-Ming Miao* and Wei-Hsin Sun†
National Defense University, Tao-Yuan 355, Taiwan, Republic of China
and
Chang-Hsien Tai‡
National Pingtung University of Science and Technology, Pingtung 912, Taiwan, Republic of China

DOI: 10.2514/1.43181

This study explores the effect of chordwise flexible deformation on unsteady aerodynamic characteristics for biplane counter-flapping dual NACA0014 airfoils with various combinations of Reynolds number and reduced frequency. Unsteady laminar viscous flows over duel rigid and flexible airfoils executing counter-plunge motion are computed with time-dependent two-dimensional laminar Reynolds-averaged Navier–Stokes equations coupled with conformal hybrid meshes. The tested Reynolds number with an airfoil characteristic chord length is 10^2, 10^3, and 10^4, and the reduced frequency ranges from 0.5 to 3.5. The dynamic mesh technique is applied to illustrate the flapping deformation modes of the flexible airfoils. To investigate the influence of the chordwise flexure extent on the aerodynamic performance of the flapping airfoils, the present study considers various different curvature deformations of flapping foils with flexure extent ranging from 0 to 0.3 times the chord length at 0.05 intervals. The visualized particle-tracing paths clearly revealed the formation and evolution of leading-edge vortices along the body of the flexible airfoil as it undergoes biplane counter-plunge motion. The generation of thrust-indicative wake structure or the drag-indicated wake structure behind the flexible airfoils depended on the degree of flexure extent of the airfoil at a fixed range of reduced frequency. The thrust force for each airfoil with biplane counter-flapping mode will be enhanced 6.32% more than that for a rigid single flapping airfoil. Present results show that flexible airfoils with flexure extent 0.25 times the chord length in counter-plunge flapping motion could get maximum propulsive efficiency and produce about 64.65% more than that of biplane rigid airfoils. The outcome indicates that appropriate flexible biplane flapping flight could not only increase the thrust force, but also boost the propulsive performance.

Nomenclature

a_o	=	flexure amplitude of the airfoil
C_d	=	drag coefficient
C_l	=	lift coefficient
c	=	chordwise length of the airfoil
F_n	=	force normal to the surface of the airfoil
F_x	=	x direction force on the surface of the airfoil
$\bar{F}_x$	=	period-averaged thrust force
f	=	flapping frequency
h	=	instantaneous plunge position
h_o	=	nondimensional plunge amplitude
k_r	=	reduced frequency, $\omega c/U_\infty$
Re	=	Reynolds number, $\rho U_\infty c/\mu$
$\bar{P}$	=	period-averaged consumption power rate
St	=	Strouhal number, $2h_o f/U_\infty$
T	=	flapping period, $2\pi/\omega$
t	=	dimensional time
t'	=	nondimensional time, tU_∞/c
U_∞	=	freestream velocity
x, y	=	Cartesian coordinate axis
δ	=	period-averaged input-power coefficient
η	=	propulsive efficiency, ξ/δ
ξ	=	period-averaged thrust-power coefficient
ρ	=	density of fluid
ψ	=	phase angle between plunging and flexing of the airfoil
ω	=	circular frequency of flapping oscillations, $2\pi f$

Presented as Paper 3817 at the 38th Fluid Dynamics Conference and Exhibit, Seattle, WA, 23–26 June 2008; received 12 January 2009; revision received 12 June 2009; accepted for publication 17 May 2009.

*Professor, Department of Mechatronic, Energy and Aerospace Engineering, Chung Cheng Institute of Technology; jmmiao@ccit.edu.tw.
†Ph.D. Student, Graduate School of Defense Science Studies, Chung Cheng Institute of Technology.
‡Professor, Department of Vehicle Engineering.

I. Introduction

THE flapping flight of birds and insects has fascinated biological scientists and researchers for hundreds of years. Many examples can be found in nature of winged creatures exhibiting excellent aerodynamic characteristics, and the flying capabilities of these creatures surpass those manifested by man-made aircraft. The outstanding flying performance of birds and insects to take off, land, hover, etc., via flapping mode has inspired researchers and engineers to think of equipping aircraft with flapping mechanisms rather than rotating propellers as a means of generating thrust and lift forces. Researchers focused on the low-Reynolds-number lift force and propulsive capability of flapping wings in hovering mode or forward-flight mode. Both experimental and numerical investigations on the kinematics, dynamics, and unsteady aerodynamic characteristics of 2-D/3-D flapping wings can be found in the recent open literature. For example, Ellington [1] pointed out that the classical steady-state model is not a practical tool to predict aerodynamic forces in flapping flight, because the calculated lift force during a cycle is not sufficient to sustain the weight of insects/birds even in forward-flight mode. Tang et al. [2] confirmed that the unsteady-force-generation mechanism is strongly related to the flapping paths of wings during upstroke and downstroke periods. To understand the unsteady-lift-generation mechanisms, such as clap-and-fling mechanism, delay dynamic stall associated with large scale of leading-edge vortices, fast pitch-up rotation, and wake capturing, several studies either in wind tunnels or by directly solving the time-dependent Navier–

Stokes equations have been conducted by three-dimensional wings or two-dimensional airfoils with hovering models [3–5].

According to biomimetic principles, some researchers had already designed flapping mini-aircraft flying in the air. Other than the consideration of the weight of a mini-aircraft, the efficiency of flapping is another quite important issue for improving flight performance due to limited energy storage. The poor aerodynamic characteristics are a predicament for minifying the size of aircraft and prolonging the time aloft in space. Although something mysterious in flapping flight is still unrevealed, the application of flapping wings had already been actively made in wind and water energy conversion plants in recent years. Moreover, a significant development related to the aviation field is the appearance of civilian and military micro aviation vehicles applications in recent decades. The Defense Air-Borne Reconnaissance Office supports a Defense Advanced Research Projects Agency initiative to develop a micro aerial vehicle (MAV), defined as a miniature remote-controlled aircraft with a wingspan of 6 in. (15 cm) or less and a flight speed of 30–60 km/h (i.e., 8.33–16.67 m/s) while carrying a miniaturized payload, simple avionics, and a communication link. The MAV would be ideal for employment by small mobile units operating in environments such as urban areas or unconventional operations anywhere. At the same time, the MAV presents a high complexity of technical challenges, as the sub-15-cm regime involves tricky changes in aerodynamics and flight control. The study of the flying techniques of small birds and insects will contribute to MAV development.

Some MAV designs use propellers as the propulsive system to generate the necessary thrust, and the passage of airstream over fixed rigid wings generates lift as a result of the pressure difference generated between the upper and lower wing surfaces. However, from a low-Reynolds-number aerodynamics perspective, flapping-wing propulsion systems are more efficient than their conventional rotational propeller counterparts (Tuncer and Kaya [6]). Murray and Howle [7] conducted their research with a flexible oscillating thin airfoil and found that the flexible airfoils may produce larger aerodynamic efficiency than rigid airfoils. Tang et al. [8] performed the fluid–structure coupling simulations on the aerodynamic characteristics of flexible airfoils in plunge and pitching motions. They found that the aerodynamic lift-force behavior of flexible airfoils is different from that of rigid airfoils. This is because the deformation of the airfoil body acts as a passive pitching motion, causing a change in the effective angle of attack, and thereafter damps the lift fluctuation during a flapping cycle. Moreover, the requirements of military planners for a MAV capable of hovering and maneuvering stably in confined spaces to perform a remote reconnaissance role, while also having the ability to take off and land on a variety of terrains, are driving researchers to investigate efficient flapping-wing propulsive technologies. One of the successful examples was performed by Jones et al. [9], who developed the flapping-wing-propelled radio-controlled MAV with a pair of counter-flapping aft airfoils to produce the thrust force.

Owing to the high interest in biomimetic propulsion, the published open literature now contains many experimental and computational investigations of the propulsion characteristics of flapping airfoils or wings. In general, these studies aim to evaluate the effects of the amplitude and frequency of the flapping motion on the generated propulsive efficiency and thrust for various shapes of the airfoil or wing. The wake vortex patterns under different reduced frequencies for an oscillating NACA0012 airfoil were reported by Lai and Platzer [10] and Jones et al. [11] in a water tunnel. To maximize the propulsion efficiency, Anderson et al. [12] found that the phase angle between the pitch and the plunge of an oscillating airfoil plays a significant role with a sinusoidal path. Read et al. [13] performed investigation on the effects of the heave amplitude, Strouhal number, effective angle of attack, and phase angle between the heave and the pitch motion on the propulsive and maneuvering behaviors of an oscillating NACA0012 airfoil under harmonic motion. Most studies controlled the airfoil in flapping mode with a path function of sinusoidal form. Hover et al. [14] intended to precisely control the optimal profile of the airfoil angle of attack rather than simply adopting a harmonic profile. They indicated that a significant

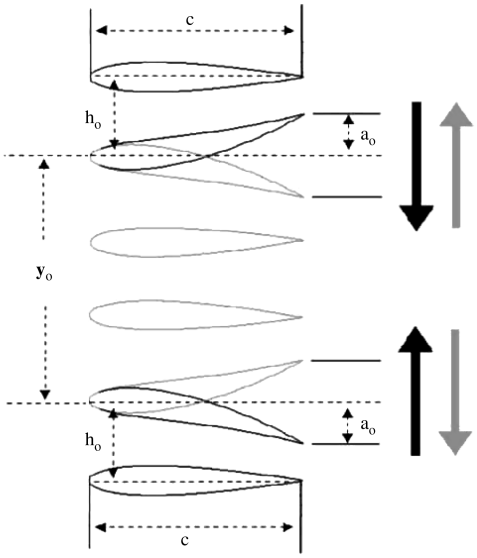

Fig. 1 Illustration of biplane counter-flapping for flexible dual airfoils.

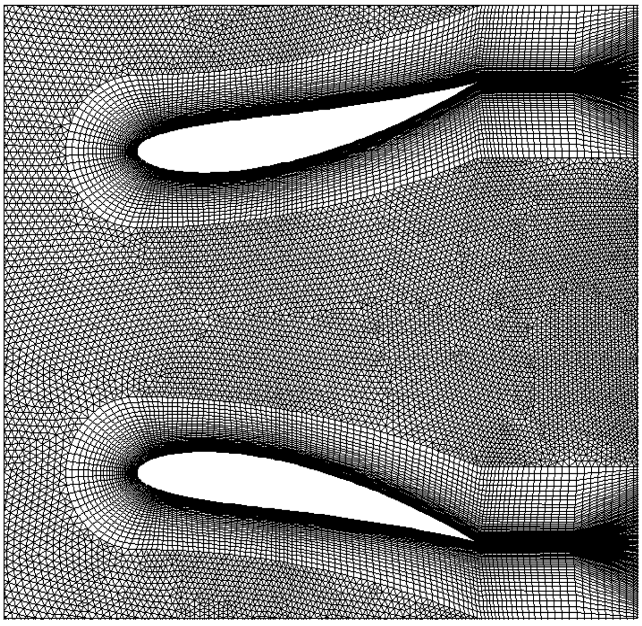

Fig. 2 Close-up illustration of conformal hybrid meshes for airfoils with flexural extent $a_0 = 0.25$.

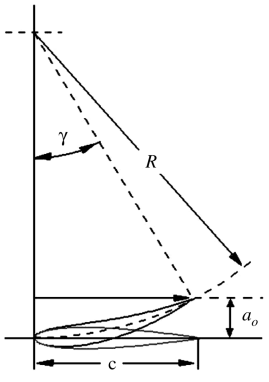

Fig. 3 Flexure pattern for flapping airfoils.

increase in the thrust and propulsion efficiency of the airfoil could be achieved by explicitly controlling the angle-of-attack profile. The highest thrust coefficient was obtained when the prescribed motion of the airfoil was performed with a sawtooth angle of attack. Heathcote et al. [15], Heathcote and Gursul [16], and Heathcote et al. [17] developed a new chordwise or spanwise flexible airfoil model and tested the effect of the airfoil stiffness on thrust, lift, and propulsive efficiency at zero freestream velocity and at low Reynolds numbers. Their experimental results showed that a higher thrust/input-power ratio could be obtained from a chordwise or spanwise flexible airfoil as compared with that for a rigid airfoil.

Numerical simulations have focused on the aerodynamic characteristic of a single rigid airfoil in freestream by solving the unsteady time-dependent Navier–Stokes equations with oscillation mode of pure pitch (Tuncer and Platzer [18]) or coupled heave and pitch (Isogai et al. [19], Isaac et al. [20], and Chandar and Damodaran, [21]). Tuncer and Kaya [22] predicted the thrust, lift, and propulsion efficiency of counter-plunge flapping wings in a biplane configuration using moving overset grids. They found that the thrust enhancement identified for flapping wings in a biplane configuration was attributed to the suppression of large-scale leading- and trailing-edge vortices by a combined pitch and plunge motion separated by an appropriate phase shift. They also intended to optimize the flapping motion of a single NACA0012 airfoil for maximum thrust and propulsion efficiency from computational fluid dynamics (CFD) data based on the steepest-ascent method. Kaya et al. [23] further extended their study on the optimization of maximum thrust performance of flapping airfoils in a biplane configuration with an aeroelastic model. As for the behavior of a flexible single airfoil executing flapping motion, Miao and Ho [24] also obtained an important conclusion via CFD method: that flexible flapping single airfoils could obtain higher propulsion efficiency than rigid airfoils.

The published open literature contains only a few studies about the unsteady aerodynamic behavior of a dual flexible airfoil executing flapping motion (see Miao sand Ho [24] and Warkentin and DeLauier [25]). Consequently, the present study computes the unsteady viscous flows over biplane counter-plunge dual NACA0014 airfoils with various chordwise flexure extents (shown in Fig. 1) by solving the incompressible Navier–Stokes equations using conformal hybrid grids. The dynamic deformable mesh technique is adopted to demonstrate the effect of the flexure extent on the unsteady aerodynamic characteristics of the flapping airfoil as it undergoes plunge oscillation. The computed flowfields around the flapping airfoils are analyzed in terms of the unsteady history of aerodynamic lift/thrust coefficients and unsteady vorticity contours and massless particle traces. The influence of the flexure extent of the airfoil on the generated thrust and propulsion efficiency are also established and discussed for flow conditions of $Re = 10^2$ to 10^4 and $k_r = 0.5$ to 3.

II. Numerical Methodology

A. Navier–Stokes Solver

This study predicts the effects of Reynolds number and reduced frequency on the development of two-dimensional unsteady viscous

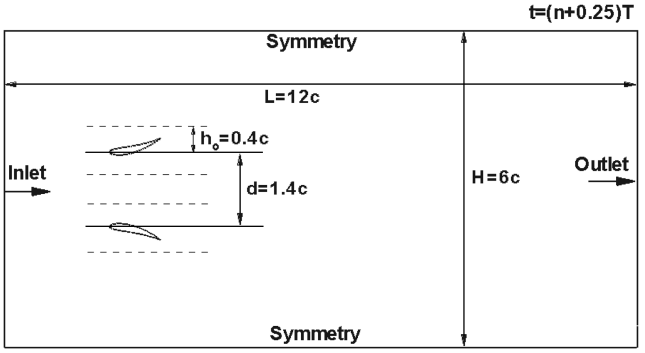

Fig. 4 Computational domain for counter-flapping flexible dual airfoils.

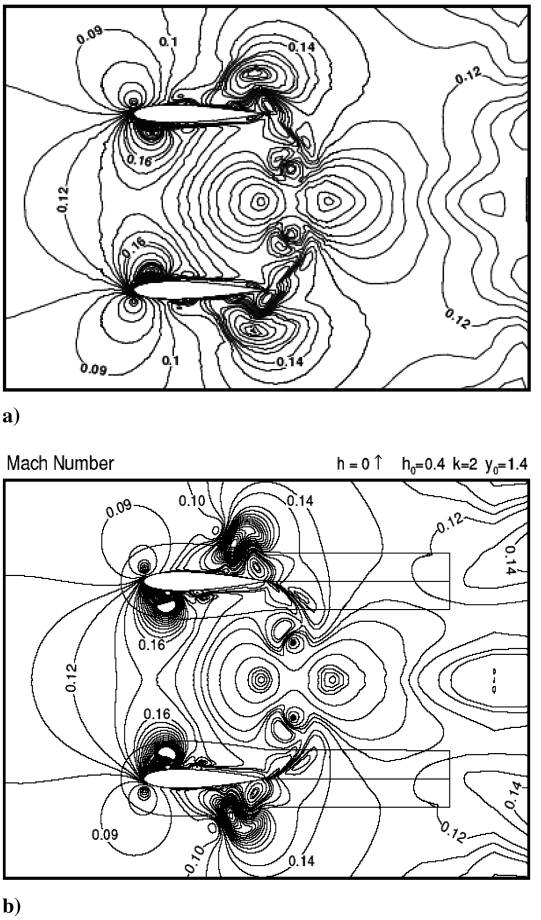

Fig. 5 Comparison between the predicted iso-Mach number contours and the results of Tuncer and Kaya [22].

flowfields induced from the interaction of free airstream and counter-flapping airfoils through conformal hybrid grid systems and dynamic mesh technique. The working fluid is air and the flowfield is assumed to be incompressible and laminar with constant thermophysical properties. The governing equations are the time-dependent incompressible Reynolds-averaged Navier–Stokes equations, including the continuity equation and momentum equation as

$$\frac{\partial \rho}{\partial t} + \rho(\nabla \cdot \vec{u}) = 0 \tag{1}$$

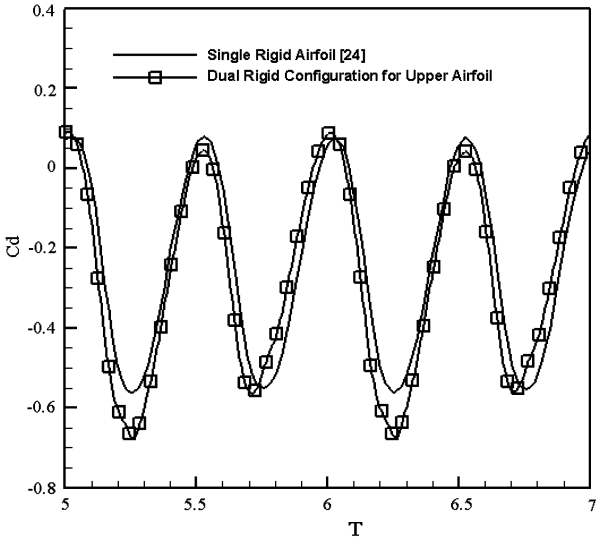

Fig. 6 Time variation of drag coefficient for single rigid airfoil [24] and dual rigid airfoils for flow condition of $Re = 10^4$, $k_r = 2$, and $h_o = 0.4$.

$$\rho\frac{\partial\vec{u}}{\partial t}+(\rho\vec{u}\cdot\nabla)\mathbf{u}=-\nabla p+\mu\nabla^2 u \tag{2}$$

The flow variables in the computational domain during the cyclical plunge motions of dual airfoils are solved with the FLUENT version 6.3.26 software based on the control volume method. The staggered unsteady-pressure-based solver is selected because the flowfield is assumed as incompressible unsteady flow. The convective flux and diffusive flux terms in governing equations are evaluated using the third-order-accurate quadratic upwind interpolation of convective kinematics scheme and the second-order-accurate central-difference scheme, respectively. The coupling between the pressure and the velocity in momentum equations is achieved by means of the PISO algorithm. An algebraic multigrid scheme is used to accelerate the convergence of scalar variables at each time interval. Because of the constraint of the hybrid mesh system, only the first-order accuracy in time can be performed for all runs. The implicit residual smoothing approach is also applied to accelerate the convergence in solutions within each physical time step. To model the flapping motion of the counter-plunge airfoils with various flexure amplitudes, the present study adopts the deformable dynamic mesh technique instead of the overset grid technique. In addition, the temporal grid deformation is governed by the geometric conservation law in each time interval.

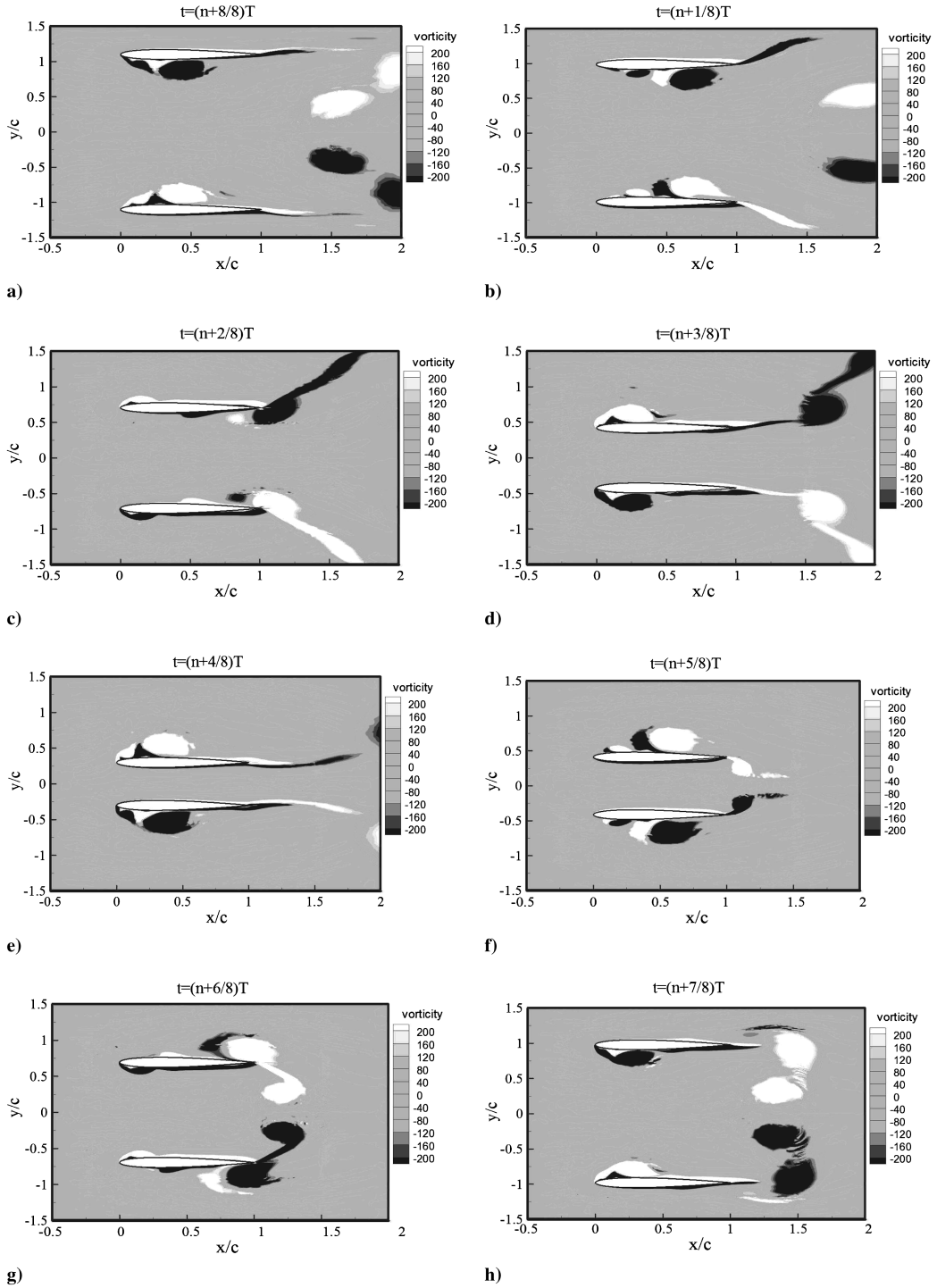

Fig. 7 Vorticity contour for dual rigid airfoils for flow condition of $Re = 10^4$, $k_r = 2$, and $h_o = 0.4$: clockwise vortices (white) and counterclockwise vortices (black).

B. Computational Grids and Boundary Conditions

Two types of grid systems, overset grids and conformal hybrid grids, are widely applied in the simulations of flapping motion of the airfoils. Isogai et al. [19] and Tuncer and Kaya [22] both used overset grids to obtain reasonable solutions for a single rigid flapping airfoil with different combinations of reduced frequency and amplitude. Because the present study aims to investigate the chordwise flexure extent of the airfoil on the propulsion efficiency under counter-plunge flapping motion with various kinetic parameters, the deformable dynamic mesh is adopted. Figure 2 is a close-up illustration to present the conformal hybrid mesh system employed for the biplane counter-flapping flexible airfoils under consideration. Following grid refinement studies, the final computational domain is composed of 21,070 inner quadrilateral cells and 43,837 outer triangular cells. The double-C-type quadrilateral cells are used to encompass the entire pair of counter-flapping airfoils, and the dynamic stretch and compression-layer mesh method is applied to model both the temporal surface and space grid deformations dominated by external user-defined functions (compiled with the C language program) during counter-plunge flapping motion for airfoils with various flexure amplitudes. The distributions of the outer triangular cells are reconstructed according to the relative position of the flapping airfoil. The interface between the quadrilateral cells and the triangular cells is modeled by conformal-type cells to ensure the conservation of flux for all variables. Both the inner quadrilateral cells and the outer triangular cells are regenerated at each time interval during simulations.

The present study intends to simulate the unsteady aerodynamic characteristics of dual NACA0014 airfoils with different flexure-amplitude deformations as it executes counter-plunge motion. The plunge motion of the airfoil shown in Fig. 1 is expressed by

$$h = \pm h_o \cos(2\pi f t) \tag{3}$$

where h denotes the instantaneous position of the airfoil, h_o denotes the half-stroke amplitude, and f denotes the flapping frequency of the airfoil. The positive and negative signals in Eq. (1) are used for the lower and upper airfoils, respectively. The initial angles of attack for dual airfoils are both set to 0 deg for present work.

We assumed that the profile of the flapping flexible airfoil in the chordwise direction continuously varies over time and is calculated by two simultaneous equations as follows:

$$R\gamma = c \tag{4}$$

$$R(1 - \cos\gamma) = ca_o \tag{5}$$

where a_o denotes the flexure extent of the airfoil (see Fig. 3), R denotes the radius of curvature, and γ represents the flexure angle. R and γ could be obtained by numerical coupling iterations for a variety of a_o. The value of the radius of curvature R corresponding the tested ranged of a_o from 0.0 to 0.3 with an interval of 0.1, is ∞, $4.893c$, $2.466c$, and $1.614c$.

Figure 4 shows that the computing domain is composed of $H = 6c$ and $L = 12c$, where c denotes the chord length of the airfoil. The spacing between the leading edges of the upper and lower airfoils at the initial instant of one complete stroke cycle is fixed at 1.4 times the chord length. The plunge amplitude for a half-stroke is 0.4 times the chord length. The dash lines shown in Fig. 4 indicate the end positions of flapping dual airfoils in the clapping-stroke and the departing-stroke periods. The instantaneous flow velocity on the flexible airfoil's boundaries in the domain must be equal to the local surface velocity described by the plunge and flexure motions of the flapping airfoil. A nonslip boundary condition is imposed on the airfoil surfaces. Inflow and outflow boundary conditions are imposed on the left and right boundary faces, respectively. The up and down faces are treated as symmetry boundaries. Freestream uniform velocity and zero-static-pressure conditions are defined at the inflow boundary and outflow boundary, respectively. The reference operational pressure is taken as 1 atm. There are two physical velocities appearing in flowfield simulations: one is the freestream air velocity and the other is the translation velocity of the flapping airfoil. Because the present study focuses on the thrust force generated from the dynamic shedding of leading-edge vortices and trailing-edge vortices on flapping airfoils, the characteristic velocity in the definition of the Reynolds number is selected as the freestream air velocity. The aerodynamic lift and drag coefficients are also normalized with freestream velocity. In general, it is found that a periodic aerodynamic solution is obtained after the fifth to the tenth cycles of time iterations in counter-flapping motion. The solution is considered to have converged satisfactorily when the difference between the thrust coefficient and propulsion efficiency values generated in successive cycles of iterations is less than 0.1%.

The aerodynamic performance of a flexible flapping airfoil can be evaluated by means of two fundamental indexes: namely, the magnitude of the thrust produced by the airfoil when in motion with various flexible flapping modes and the input power, which is defined as the total consumptive work required generating the plunge and deflection motions of the airfoil. The propulsion efficiency of an airfoil can be defined as the ratio of the propulsion power to the input power. This ratio provides a meaningful index when attempting to optimize the propulsive aerodynamic performance by considering airfoils of different chordwise flexure amplitudes. The present work

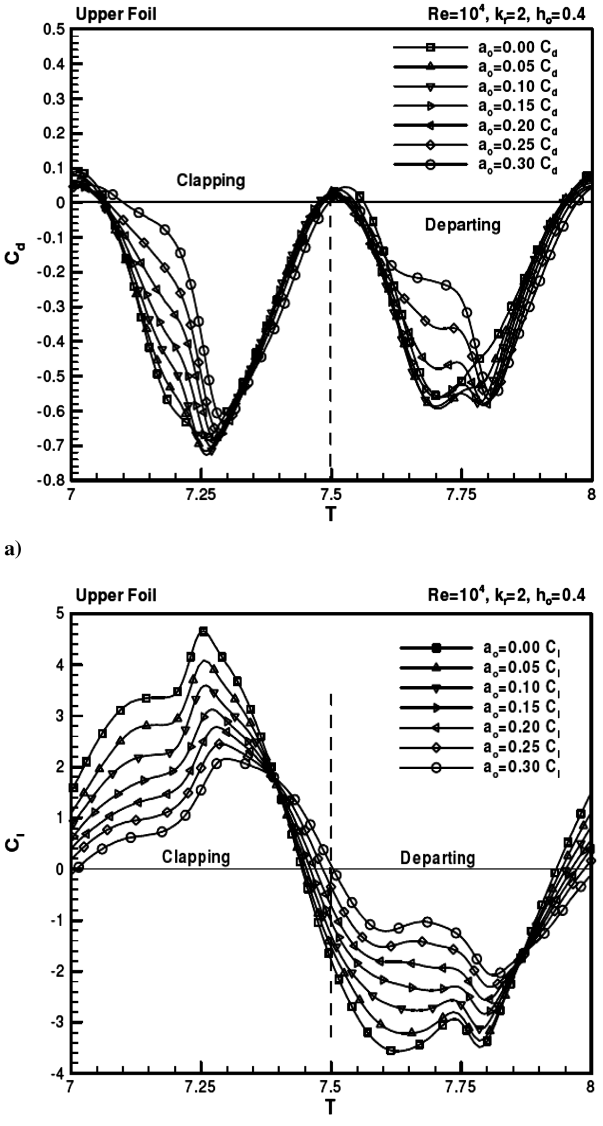

Fig. 8 Time variation of C_d and C_l values under different flexure extent for flow condition of $Re = 10^4$, $k_r = 2$, and $h_o = 0.4$.

considers a flexible airfoil with a chord length c moving at a constant forward velocity U_∞ and performing a harmonic plunge motion $h(t)$ of an amplitude h_o and a frequency f. If T denotes the period of oscillation in the positions of the airfoils, the predicted period-averaged consumption power rate $\bar{P}$ and the thrust force $\bar{F}_x$ can be evaluated, respectively, as

$$\bar{P} = \frac{1}{T}\int_0^T F_n(t)\,\frac{\mathrm{d}S_n}{\mathrm{d}t}, \qquad \bar{F}_x = \frac{1}{T}\int_0^T F_x(t)\,\mathrm{d}t \tag{6}$$

where $F_n(t)$ and $F_x(t)$ represent the instantaneous generated force components in the normal direction and the x direction of the airfoil surfaces, respectively. The term $\mathrm{d}S_n/\mathrm{d}t$ denotes the traveling velocity of the flexible airfoil as it executes the plunge motion.

The period-averaged consumption power rate is expressed in a nondimensional form and is defined as the period-averaged input-power coefficient δ; that is,

$$\delta = \frac{\bar{P}}{(\frac{1}{2}\rho U_\infty^2 cs)U_\infty} \tag{7}$$

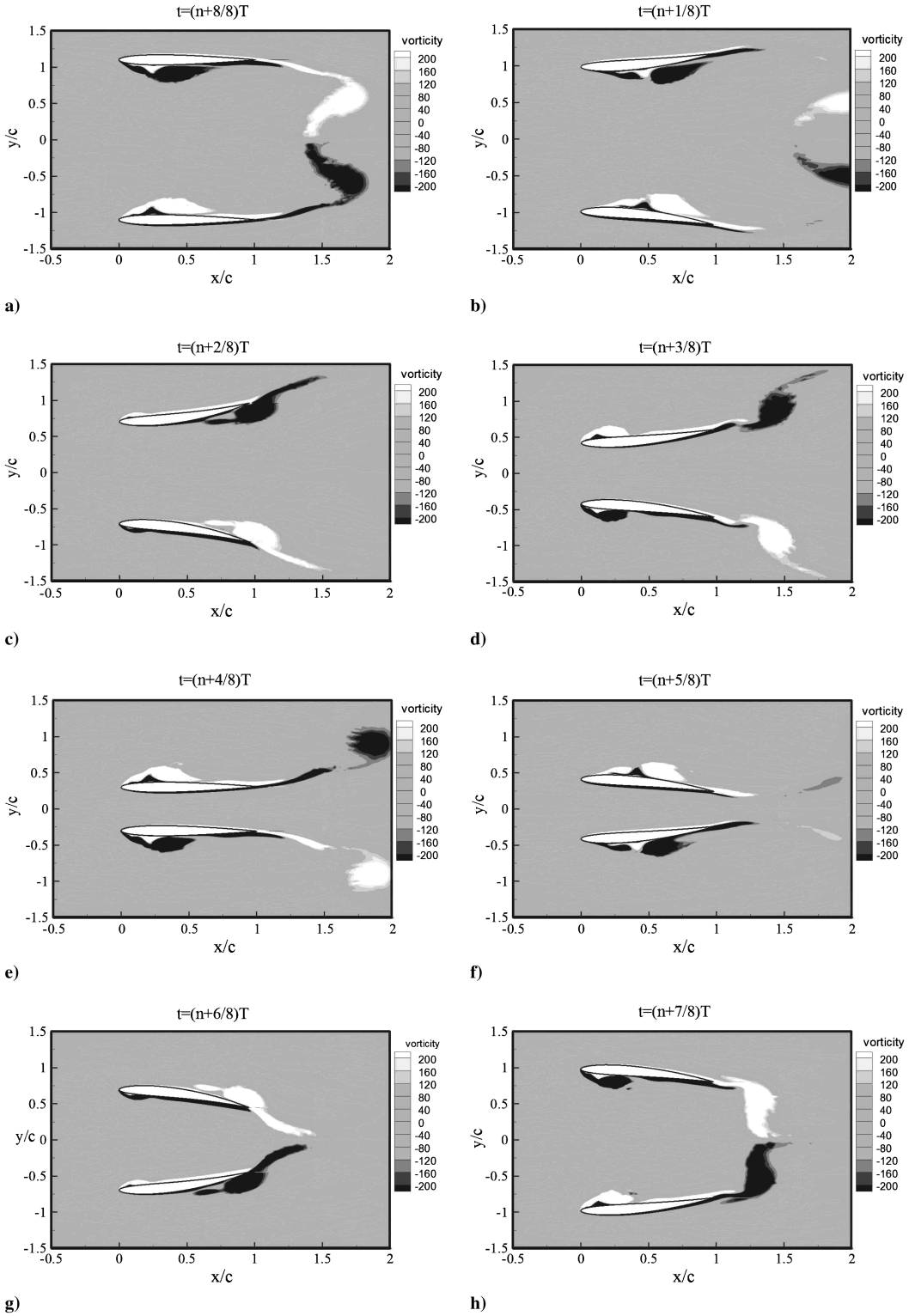

Fig. 9 Vorticity contour for dual flexible airfoils with $a_0 = 0.25$ for flow condition of $Re = 10^4$, $k_r = 2$, and $h_o = 0.4$: clockwise vortices (white) and counterclockwise vortices (black).

The symbol ξ is defined as the period-averaged thrust-power coefficient and is expressed as

$$\zeta = \frac{1}{T}\int_0^T (-C_d)\,\mathrm{d}t \tag{8}$$

where C_d is the instantaneous drag coefficient. Therefore, the propulsion efficiency η of flapping airfoils with plunge motion is defined as

$$\eta = \frac{\xi}{\delta} \tag{9}$$

III. Results and Discussion

To validate the computer code in unsteady and incompressible low-Reynolds-number flowfield simulations, the present study performed a preliminary run on biplane flapping rigid NACA0014 airfoils for flow conditions of $Re = 10^4$, $k_r = 2$, and $h_o = 0.4$. Figure 5a shows the predicted iso-Mach-number contour flowfield when the dual airfoils are moved toward each other at the beginning instant of the clapping stroke. The numerical result with overset grid system from Tuncer and Kaya [22] is also presented in Fig. 5b for comparison. As expected, the predicted flowfield is symmetrical with respect to the middle line between airfoils. Moreover, the evaluations of the leading-edge vortex (LEV) and the trailing-edge vortex (TEV)

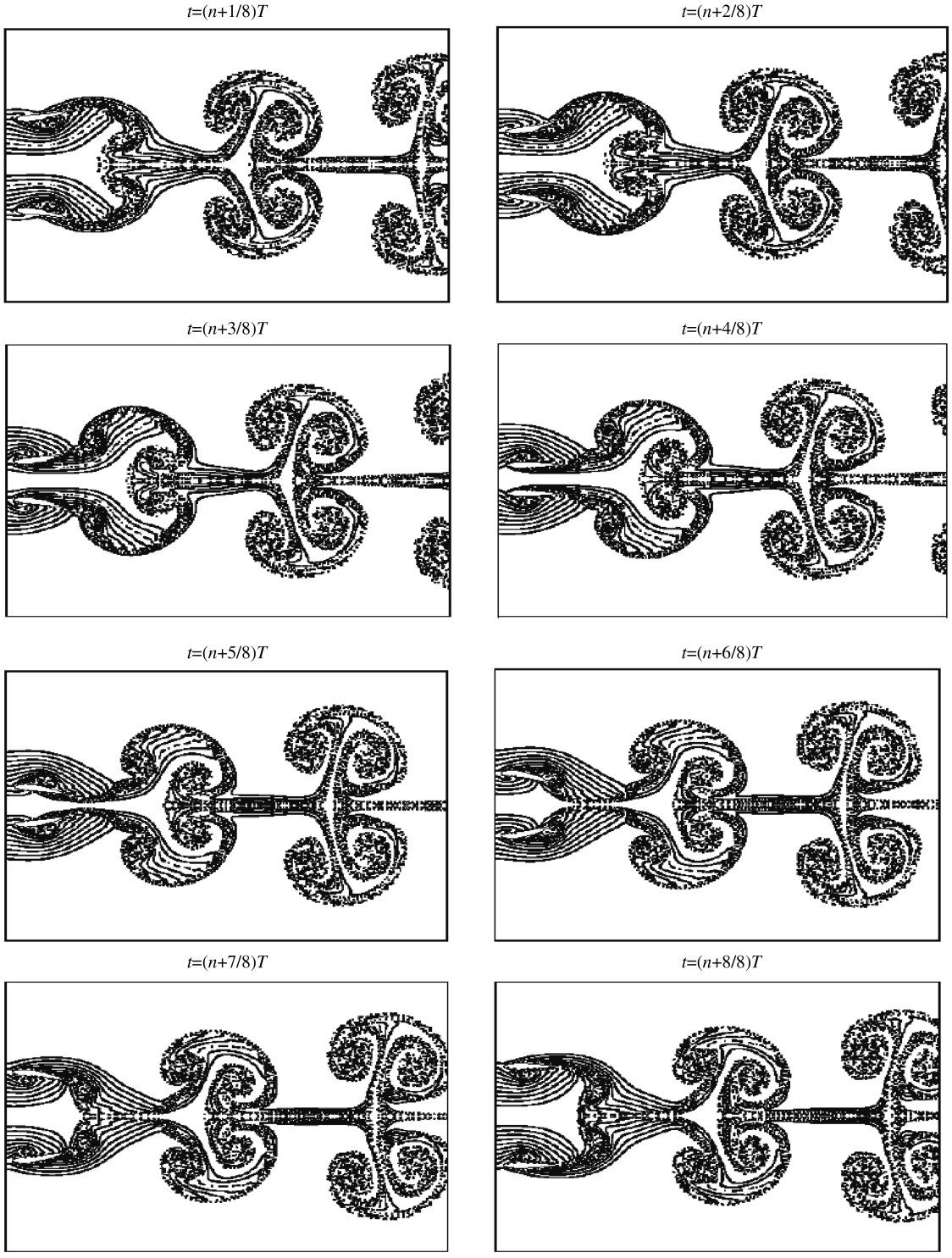

Fig. 10 Instantaneous particle traces along a period of the airfoil with $a_o = 0.25$ for flow condition of $Re = 10^4$, $k_r = 2$, and $h_o = 0.4$.

around the outer and inner sides of the dual airfoils are clearly observed and both agree well with those of Tuncer and Kaya [22]. To explore the effect of the counter-flapping mode on the aerodynamic performance, the present study specified values of $Re = 10^4$, $k_r = 2$, and $h_o = 0.4$ and computed the time variations of the aerodynamic coefficient for a single rigid airfoil [24] and counter-flapping dual rigid airfoils. The predicted curves of drag coefficient with respect to flow time are presented in Fig. 6. Regardless of the single- or dual-airfoil configuration, the time history of drag coefficient for pure plunge motion both exhibited cycling variations, which is linked to the predefined sinusoidal flapping paths of the airfoils. For dual rigid airfoils, the drag coefficient distribution agrees well with that of Tuncer and Kaya [22].

The instant vorticity contours for dual rigid airfoils over a complete cycle under the same flow conditions are plotted in Fig. 7 for the discussion of the unsteady flow mechanism. When the upper and lower airfoils reach the end positions of flapping stroke (i.e., $h = 0.4c \downarrow$ and $0.4c \uparrow$). Figure 7a shows that the wake structure shedding from the trailing edge of the airfoil is believed to be drag-indicative form and there is little difference between a single airfoil and dual airfoils (Fig. 6). The acceleration of the airfoils causes the attached vortex on the inner portion of the airfoils gradually moving toward the trailing edge to produce thrust force, as shown in Fig. 7b. This clapping process will enlarge the core size of the LEV (Fig. 7c), which leads to a larger suction of airstream toward the upper portion of the airfoils, to produce more thrust force. When the airfoils reach their maximum velocity, a peak thrust-force coefficient for both runs can be observed from Fig. 6. Inspection of Figs. 7b and 7c reveals that the interaction of periodic formations of LEV and in-sequence shedding TEV to downstream changes the corresponding wake structure from drag-indicative pattern to thrust-indicative pattern. With the single rigid airfoil as the reference, the peak value of the thrust force for the upper airfoil increases to 21.18% as the dual airfoils move closer to the end position of the clapping stroke. Tuncer and Kaya [22] found a similar flow mechanism from the pressure distributions over both sides of the airfoils.

In the aft part periodic of the clapping stroke (i.e., $5 + 1/4T < T < 5 + 1/2T$), the drag coefficients gradually changed from negative values to positive values and it is almost the same between single and dual airfoils in the flapping motion. The flow structure around the airfoil is complex at this time interval, as shown in Figs. 7d and 7e. Generally, the outer side of the airfoils is originally occupied with one LEV, one recirculation bubble, and a clockwise vortex near the middle chord of the airfoil (Fig. 7e). When the airfoils restart to accelerate to the maximum speed (i.e., $T = 5 + 3/4T$), Fig. 6 shows that the thrust force is regenerated in this period. The vorticity contours (Figs. 7f and 7g) clearly exhibit that the two pairs of vortex structures are formed and gradually move to the trailing edge. Finally, these vortices are shed downstream with a fixed tilt angle to form a mushroom pattern. In the meantime, a new LEV is formed in the inner side of the airfoils. Moreover, Fig. 6 shows that there is little difference in generating maximum thrust force in the period of the departing stroke among tested cases. As the airfoil further decelerates to its initial position, the combination of the high- and low-pressure areas leads to an increase of drag force at the aft part periodic of the departing stroke (Fig. 7h). Generally, it is observed that the unsteady interaction of leading-edge vortex and trailing-edge vortex around the flapping airfoils significantly affects the aerodynamics performance. This observation confirms that the low-Reynolds-number aerodynamics of flapping airfoils cannot be explained by the steady-state fluid dynamic theory, because the fluid physics is definitely time-dependent. It should also be noted that this distribution in thrust force over a complete cycle of flapping motion will lead to a variation of the total input power.

Figure 8 shows the predicted time history of C_d and C_l values over a complete cycle for the upper flapping airfoil with different flexure extents under a flow condition of $Re = 10^4$, $k_r = 2$, and $h_o = 0.4$. The corresponding vorticity contours and particle traces for dual-airfoil configuration with a flexure extent of $0.25c$ are displayed in Figs. 9 and 10, respectively. Inspection of Fig. 8a reveals that the effect of the flexure extent of the airfoil on the drag coefficient history obviously occurs on the acceleration stage of the clapping and departing strokes. The thrust force from the flapping airfoils is decreased with increasing of flexure extent among the tested cases. This is due to the fact that the thrust-indicative wake pattern is formed from the interaction of the separating leading-edge vortex with the trailing-edge vortex. The deformation of the airfoil shape on the trailing edge will reduce this vortex-vortex interaction (Fig. 9). However, there is little difference in thrust-force history when the airfoils move from the maximum speed to the rest condition. Observation of the vorticity contours shows that the formation of the leading-edge vortex, the associated attached separation bubble, and the clockwise rotation vortex near the middle of the airfoil are less influenced by the degree of flexure extent in this deceleration period. For the counter-flapping dual-airfoil configurations, the effect of the chordwise flexure extent on the thrust force is exhibited of twin peaks instead of the single peak at the middle of the departing stroke. Figure 8b shows that the positive lift force is generated in the clapping stroke but the negative lift force is generated in the departing stroke, which is attributed to the dynamic stall effect. In addition, the effect of flexure extent on the lift coefficient is opposite to that of the drag coefficient for a dual-flexible-airfoil configuration with plunge oscillation.

The flow mechanism of thrust-force generation for the biplane counter-flapping dual-airfoil configuration can be further examined from the observation of particle traces over a complete cycle, as shown in Fig. 10. Some major features on the complex unsteady wake structure can be classified. Placing massless particles at the upstream positions of the leading edge of the dual airfoils, the aforementioned cyclic mutual interaction of the separating leading-edge vortex with the trailing-edge vortex over a complete cycle results in the formations of a mushroom pattern of the wake structure. The mushroom pattern of particle traces is symmetrical with respect to the central line of the airfoils, because the counter-flapping motion is specified. The mushroom heads point downstream, meaning that the thrust force is generated during cyclic oscillation of the airfoils. The experimental study by Lai and Plazter [10] found a similar flow pattern of wake structure for a plunging airfoil. The present study found that the wake structure is a function of not only Reynolds number but also the flexure extent of the airfoil at a fixed reduced frequency that characterizes the propulsion efficiency of the dual airfoils.

Figure 11 shows the variations of the input-power coefficient δ, the period-averaged thrust-power coefficient ζ, and the propulsion efficiency η with respect to the flexure extent of the airfoil for flow conditions of $Re = 10^4$, $k_r = 2$, and $h_o = 0.4$. The predicted result for a single airfoil with the same flapping mode is also presented for comparison. The maximum period-averaged thrust force occurs for a flexure extent of 0.1, which is similar to the earlier observation for a single airfoil [24]. Meanwhile, the period-averaged thrust force is

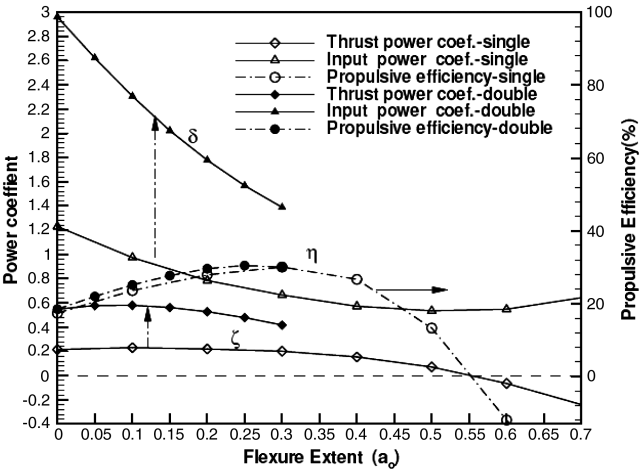

Fig. 11 Interrelationship between the input-power coefficient, trust power coefficient and propulsive efficiency with respect to flexure extent computed at $Re = 10^4$, $k_r = 2$, and $h_o = 0.4$.

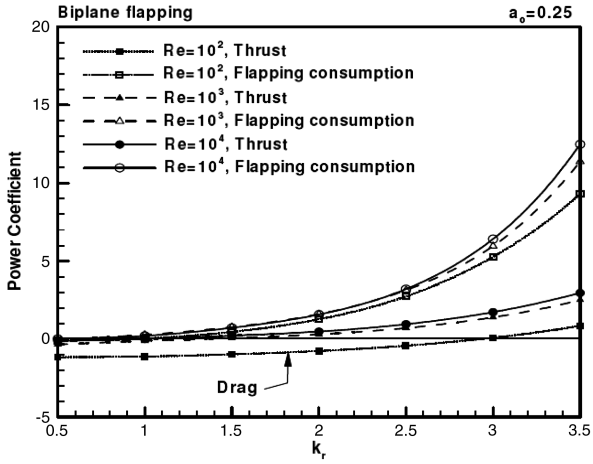

Fig. 12 Effect of reduced frequency on power coefficient at $Re = 10^2$, 10^3, and 10^4.

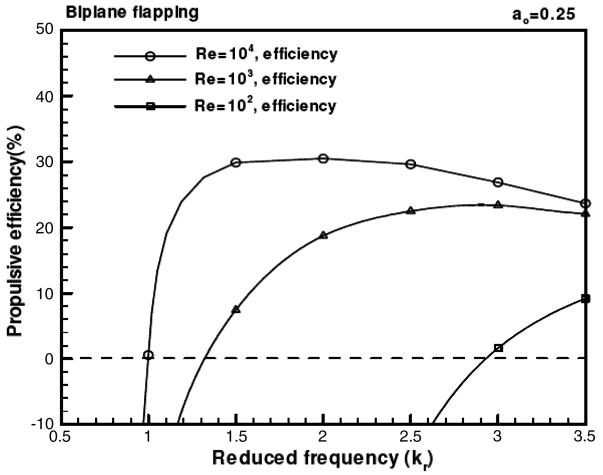

Fig. 14 Effect of reduced frequency on propulsive efficiency at $Re = 10^2$, 10^3, and 10^4.

increased 2.52 times. Increase of the flexure extent of the airfoil from 0.1 to 0.3 results in the decay of period-averaged thrust force. The relationship between the input-power coefficient with flexure extent of the airfoil is monotonically descending. Furthermore, it can be seen that the trend in the propulsive efficiency with increasing flexure amplitude is not monotonic.

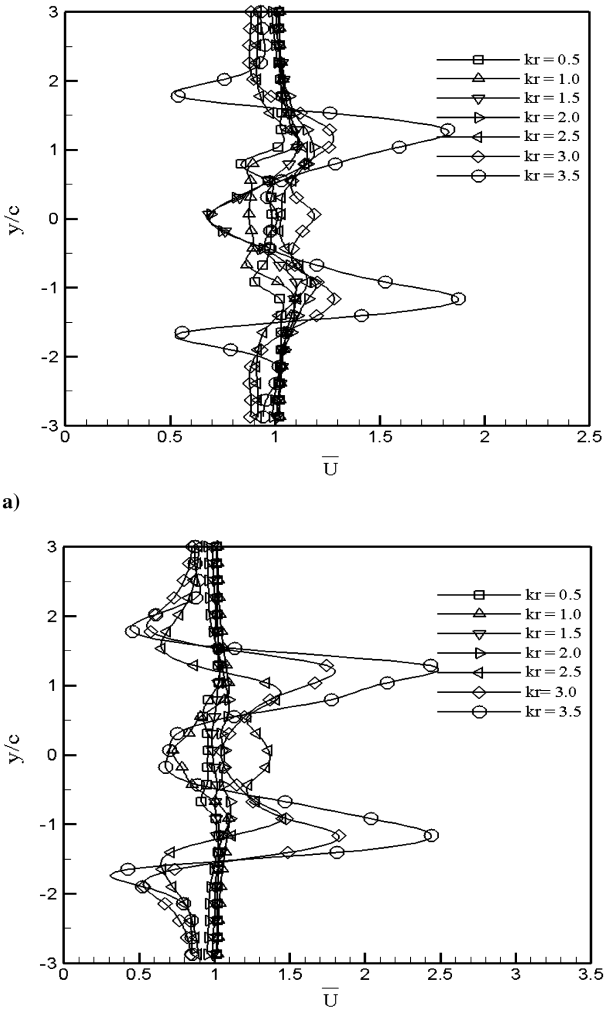

Fig. 13 Effect of reduced frequency on downstream period-averaged mean velocity-magnitude distribution for dual flexible airfoils with $a_0 = 0.25$ in cases of $Re = 10^4$ and $h_o = 0.4$: a) $x/c = 1.0$ and b) $x/c = 1.5$.

This study also investigates the effects of the Reynolds number and the reduced frequency on the aerodynamic performance of a flapping airfoil with the flexure amplitude of 0.25. Note that the nondimensional plunge amplitude is maintained at a constant of $h_o = 0.4$ in all runs. Figure 12 presents the variations of the period-averaged thrust-power and input-power coefficients with the reduced frequency for frequency values of $k_r = 0.5$–3.5 and Reynolds numbers of $Re = 10^2$, 10^3, and 10^4, respectively. It can be seen that the reduced frequency value has a greater effect on the thrust-power coefficients and input-power coefficients than the Reynolds number. The thrust-power coefficient increases linearly with the reduced frequency value in the tested range of Reynolds numbers, as shown in Fig. 13. The input-power coefficient increases exponentially as the reduced frequency increases. This trend can be attributed to the fact that a more rapid oscillation of the flexible airfoil in flapping motion requires the input of a greater mechanical power. Figure 14 illustrates the influence of the reduced frequency value on the propulsive efficiency of a flexible airfoil with a flexure amplitude of $a_0 = 0.25$ at Reynolds numbers of $Re = 10^2$, 10^3, and 10^4, respectively. The overall domain is divided by the dashed line into an upper thrust-dominated zone and a lower drag-dominated zone. The reduced frequency values corresponding to the peak propulsive efficiency at Reynolds numbers of $Re = 10^2$, 10^3, and 10^4 are found to be $k_r = 3.5$, 3, and 1.5, respectively.

IV. Conclusions

A numerical investigation of counter-flapping flexible flapping dual-airfoil propulsion suitable for micro aerial vehicles (MAVs) has been accomplished. This study has employed Navier–Stokes analysis to compute the unsteady viscous flowfields associated with a low-Reynolds-number flow over a dual chordwise flexible airfoil executing in-plane plunge motion. The computational domain has been constructed with conformal hybrid meshes and the dynamic mesh technique applied to illustrate the continuous deformation modes of the flexible flapping airfoil. To ensure a comprehensive examination of the influence of the flexure amplitude on the aerodynamic performance of the flapping airfoil at $Re = 10^4$, $k_r = 2$, and $h_o = 0.4$, the present study has considered seven flexure amplitudes a_o, ranging from 0.0 to 0.3 at an interval of 0.05. The thrust-indicative mushroom pattern of wake structures have been observed behind the trailing edge of the airfoil for airfoils with flexure amplitudes of 0.0 to 0.25 times the chord length. The results have shown that the period-averaged propulsion efficiency is optimized when the flapping airfoil has a flexure extent of 0.25. This study has also computed the propulsion efficiency and the propulsion thrust under various combinations of Reynolds number and reduced frequency. The numerical results have confirmed that the propulsion efficiency is influenced primarily by the value of the reduced frequency rather than by the Reynolds number.

Acknowledgment

The financial support from National Science Council of Taiwan under contract number NSC95-2623-7-014-011-D is deeply appreciated.

References

[1] Ellington, C. P., "The Aerodynamics of Hovering Insect Flight, 1: The Quasi-Steady Analysis," *Philosophical Transactions of the Royal Society of London, Series B: Biological Sciences*, Vol. 305, No. 1122, 1984, pp. 1–15. doi:10.1098/rstb.1984.0049

[2] Tang, J., Viieru, D., and Shyy, W., "Effects of Reynolds Number and Flapping Kinematics on Hovering Aerodynamics," AIAA Paper 2007-129, Jan. 2007.

[3] Liu, H., and Kawaxhi, K., "A Numerical Study of Insect Flight," *Journal of Computational Physics*, Vol. 146, No. 1, 1998, pp. 124–156. doi:10.1006/jcph.1998.6019

[4] Sun, M., and Tang, J., "Unsteady Aerodynamic Force Generation by a Model Fruit Fly Wing in Flapping Motion," *Journal of Experimental Biology*, Vol. 205, No. 1, 2002, pp. 55–70.

[5] Wang, Z. J., Birch, J. M., and Dickinson, M. H., "Unsteady Forces and Flows in Low Reynolds Number Hovering Flight: Two-Dimensional Computations vs Robotic Wing Experiments," *Journal of Experimental Biology*, Vol. 207, No. 3, 2004, pp. 449–460. doi:10.1242/jeb.00739

[6] Tuncer, I. H., and Kaya, M., "Thrust Generation Caused by Flapping Airfoils in a Biplane Configuration," *Journal of Aircraft*, Vol. 40, No. 3, 2003, pp. 509–515. doi:10.2514/2.3124

[7] Murray, M. M., and Howle, L. E., "Spring Stiffness Influence on an Oscillation Propulsor," *Journal of Fluids and Structures*, Vol. 17, No. 7, 2003, pp. 915–926. doi:10.1016/S0889-9746(03)00026-4

[8] Tang, J., Viieru, D., and Shyy, W., "A Study of Aerodynamics of Low Reynolds Number Flexible Airfoils," AIAA Paper 2007-4212, June 2007.

[9] Jones, K. D., Bradshaw, C. J., Papadopoulos, J., and Platzer, M. F., "Bio-Inspired Design of Flapping-Wing Micro Air Vehicles," *The Aeronautical Journal*, Vol. 109, No. 1098, 2005, pp. 385–393.

[10] Lai, J. C. S., and Platzer, M. P., "The Characteristics of a Plunging Airfoil at Zero Free-Stream Velocity," *AIAA Journal*, Vol. 39, No. 3, 2001, pp. 531–534. doi:10.2514/2.1340

[11] Jones, K. D., Dohring, C. M., and Platzer, M. F., "Experimental and Computational Investigation of the Knoller-Betz Effect," *AIAA Journal*, Vol. 36, No. 7, 1998, pp. 1240–1246. doi:10.2514/2.505

[12] Anderson, J. M., Streitlen, K., Barrett, D. S., and Triantafyllou, M. S., "Oscillating Foils of High Propulsive Efficiency," *Journal of Fluid Mechanics*, Vol. 360, 1998, pp. 41–72. doi:10.1017/S0022112097008392

[13] Read, D. A., Hover, F. S., and Triantafyllou, M. S., "Forces on Oscillating Foils for Propulsion and Maneuvering," *Journal of Fluids and Structures*, Vol. 17, No. 1, 2003, pp. 163–183. doi:10.1016/S0889-9746(02)00115-9

[14] Hover, F. S., Haugsdal, O., and Triantafyllou, M. S., "Effect of Angle of Attack Profiles in Flapping Foil Propulsion," *Journal of Fluids and Structures*, Vol. 19, No. 1, 2004, pp. 37–47. doi:10.1016/j.jfluidstructs.2003.10.003

[15] Heathcote, S., Martin, D., and Gursul, I., "Flexible Flapping Airfoil Propulsion at Zero Freestream Velocity," *AIAA Journal*, Vol. 42, No. 11, 2004, pp. 2196–2204. doi:10.2514/1.5299

[16] Heathcote, S., and Gursul, I., "Flexible Flapping Airfoil Propulsion at Low Reynolds Numbers," AIAA Paper 2005-1405, Jan. 2005.

[17] Heathcote, S., Wang, Z., and Gursul, I., "Effect of Spanwise Flexibility on Flapping Wing Propulsion," *Journal of Fluids and Structures*, Vol. 24, No. 2, 2008, pp. 183–199. doi:10.1016/j.jfluidstructs.2007.08.003

[18] Tuncer, I. H., and Platzer, M. P., "Thrust Generation Due to Airfoil Flapping," *AIAA Journal*, Vol. 34, No. 2, 1996, pp. 324–331. doi:10.2514/3.13067

[19] Isogai, K., Shinmoto, Y., and Watanabe, Y., "Effects of Dynamic Stall on Propulsive Efficiency and Thrust of a Flapping Airfoil," *AIAA Journal*, Vol. 37, No. 10, 1999, pp. 1145–1151. doi:10.2514/2.589

[20] Isaac, K. M., Rolwes, J., and Colozza, A., "Aerodynamics of a Flapping and Pitching Wing Using Simulations and Experiments," *AIAA Journal*, Vol. 46, No. 6, 2008, pp. 1505–1515. doi:10.2514/1.32846

[21] Chandar, D., and Damodaran, M., "Computational Study of Unsteady Low Reynolds Number Airfoil Aerodynamics on Moving Overlapping Meshes," *AIAA Journal*, Vol. 46, No. 2, 2008, pp. 429–438. doi:10.2514/1.31499

[22] Tuncer, I. H., and Kaya, M., "Optimization of Flapping Airfoils for Maximum Thrust and Propulsive Efficiency," *AIAA Journal*, Vol. 43, No. 11, 2005, pp. 2329–2336. doi:10.2514/1.816

[23] Kaya, M., Tuncer, I. H., Jones, K. D., and Platzer, M. F., "Optimization of Aeroelastic Flapping Motion of Thin Airfoils in a Biplane Configuration for Maximum Thrust," AIAA Paper 2007-0484, Jan. 2007.

[24] Miao, J. M., and Ho, M.-H., "Effect of Flexure on Aerodynamic Propulsive Efficiency of Flapping Flexible Airfoil," *Journal of Fluids and Structures*, Vol. 22, No. 3, 2006, pp. 401–419. doi:10.1016/j.jfluidstructs.2005.11.004

[25] Warkentin, J., and DeLauier, J., "Experimental Aerodynamic Study of Tandem Flapping Membrane Wings," *Journal of Aircraft*, Vol. 44, No. 5, 2007, pp. 1653–1661. doi:10.2514/1.28160